

A method for the global optimization of the tooth contact pattern and transmission error of spiral bevel and hypoid gears^{*}

Yao-bin ZHUO^{†1,2}, Xue-yan XIANG¹, Xiao-jun ZHOU², Hao-liang LV², Guo-yang TENG²

(¹College of Engineering and Design, Lishui University, Lishui 323000, China)

(²State Key Laboratory of Fluid Power and Mechatronics Systems, Zhejiang University, Hangzhou 310027, China)

[†]E-mail: zhuoyaobin@163.com

Received Mar. 14, 2016; Revision accepted Aug. 31, 2016; Crosschecked Apr. 11, 2017

Abstract: In this paper, we present a method for the global optimization of the tooth contact pattern and transmission error of spiral bevel and hypoid gears, which includes three optimization objectives, three control parameters, and a complex-constrain genetic algorithm solving method. A new set of fundamental equations for pitch cone parameters of hypoid gear drives are established, as well as the relationships between pitch cone and curvature parameters. Based on this theory, three control parameters are selected to determine the pinion tooth surface. A hypoid gear drive is chosen for case studies. The results verify that the optimization methodology can achieve the expected optimization objectives and has good convergence. Correlations between optimization objectives and control parameters are discussed. Furthermore, a finite element model of a simplified hypoid gear drive system is established and its quasi-static meshing characteristics analyzed. The results again confirm the correctness of the optimization method. The effects of torque load on the contact pattern and transmission error are discussed. The results provide a theoretical reference for geometric calculations, quasi-static analysis, and optimal design of spiral bevel and hypoid gears.

Key words: Spiral bevel gear; Tooth contacts; Transmission error; Optimal design; Genetic algorithm; Finite element analysis
<http://dx.doi.org/10.1631/jzus.A1600240>

CLC number: TH122


1 Introduction

Spiral bevel and hypoid gears are critical components of many train power systems. They have found broad application in helicopter and truck transmissions, and reducers for transformation of rotation and torque between intersected or crossed axes (Litvin and Fuentes, 2004). Because of their geometry and manufacturing complexity, hypoid gears can be considered to be the most general case of gearing. Design and tooth contact analysis (TCA) of

such gear drives has been a topic of research by many scientists.

Although spiral bevel and hypoid gears have been widely used and analyzed, few studies have presented a comprehensive optimization method, largely due to the complex geometric structure of such gears. Litvin *et al.* (1998; 2002; 2006) and Argyris *et al.* (2002) developed the geometry, generation, and simulation of the meshing and contact of spiral bevel gears with a localized bearing contact, and proposed an approach called ‘local synthesis’ for providing a predesigned parabolic function of transmission error with limited magnitude of maximum transmission error. However, their method focused only on the characteristics of the mean contact point. Vogel *et al.* (2002) presented a constructive approach called ‘ease-off topography’ for the approximation-free TCA of hypoid bevel gears. They obtained directly the characteristics of the paths of contact, the

^{*} Project supported by the National Natural Science Foundation of China (No. 51275453), the Key Research Project of Lishui, China (No. 2016ZDYF15), the North Vehicle Research Institute, and Hangzhou Advance Gearbox Group Co., Ltd., China

 ORCID: Yao-bin ZHUO, <http://orcid.org/0000-0002-0954-9740>; Xiao-jun ZHOU, <http://orcid.org/0000-0003-2565-1398>

© Zhejiang University and Springer-Verlag Berlin Heidelberg 2017

transmission error, and the contact ellipses. Their method represents a significant step towards a systematic optimization. Using this method, Achtmann and Bär (2004) optimized bearing ellipses for the coast and drive side of hypoid gears.

Artoni *et al.* (2008; 2009) developed an approach to the automatic optimization of the loaded tooth contact pattern of spiral bevel and hypoid gears. They then proposed an optimization methodology to define systematically the optimal ease-off topography to minimize simultaneously the loaded transmission error (LTE) of hypoid gears. Mermoz *et al.* (2013) presented an optimization process, capable of automatically designing the shape of spiral bevel gear flanks, and then developed a methodology to reduce the quasi-static transmission error of the spiral bevel gears. However, none of these studies meticulously studied the combination of tooth contact pattern and transmission error.

Simon (2009a; 2009b; 2013; 2014) analyzed the influences of machine settings and tool geometry on tooth contact pressure and loaded transmission error, and presented a methodology to optimize tooth modifications in face-hobbed hypoid gears. These sensitivity studies give clues about the improvement of gear performance. Guo *et al.* (2016) presented an optimal design method for cutter blade profiles to eliminate the tooth edge contact and improve the distribution of tooth contact stress for face-hobbed spiral bevel gears in the case of heavy load and misalignment. The research introduces a multi-segment cutter blade profile with Toprem, Flankrem, and cutter tip to obtain the ideal load and contact stress distribution.

Some optimization methods for spiral bevel and hypoid gears have been developed. However, few studies have presented multi-objective synthesis optimization of tooth contact pattern and transmission error, which is a more efficient way to deal with the problem. Furthermore, control parameters and their effects on the results have seldom been considered. Therefore, we present a global optimization methodology for the tooth contact pattern and transmission error of spiral bevel and hypoid gears. The methodology contains three optimization goals, three control parameters, and a solving method based on a complex-constrain genetic algorithm. The effects of control parameters are investigated using case studies. The

finite element (FE) approach is used to verify the results.

2 Defect analysis of tooth contact pattern and transmission error

2.1 Common defects of tooth contact pattern

The traditional method for computing cutter specifications and machine settings for the manufacture of spiral bevel and hypoid gears controls only the normal vector and the curvatures of the calculated point (Shtipelman, 1978). Therefore, the calculation cannot ensure that the whole tooth contact pattern will meet expectations. Errors may lead to location, size, and shape defects of the tooth contact pattern (Shtipelman, 1978). There are numerous kinds of control parameters in the traditional method, such as the pressure angle, spiral angle, coefficient of contact zone length, pitch cone distance of generating gear, pitch angle of generating gear, offset, root angle, machine root angle, and the local synthesis calculation process. In addition, the collective and cross influences of these parameters are so complicated that they can hardly be understood and applied. Hence, these parameters are not suitable for the optimal design of meshing characteristics.

2.2 Common defects of transmission error

Unreasonable modification of machine-tool settings of the gear and the pinion will also lead to various types of transmission error curves (Fig. 1).

3 Optimization objectives

Reasonable optimization objectives are very important for the optimal design process. Based on the economic principle, which means that fewer optimization objectives restrict increase in defects, three optimization objectives are selected (Fig. 2). The real 3D contact pattern of the tooth surface is converted to the form in the gear axial section, which is helpful for subsequent analysis.

1. Semi-major axis of instantaneous contact ellipse l

The semi-axis l can effectively restrict the contact zone length and prevent the defects of wide,

narrow, long, and short contacts. The optimal value of l can be selected as

$$l_{\text{OPT}} = \frac{F \cdot b_g}{2 \cos \beta_g}, \quad (1)$$

where F is the coefficient of contact zone length, b_g the tooth width of the gear, and β_g the mean spiral angle of the gear.

There are innumerable instantaneous contact ellipses inside the cycle of meshing, and each of their

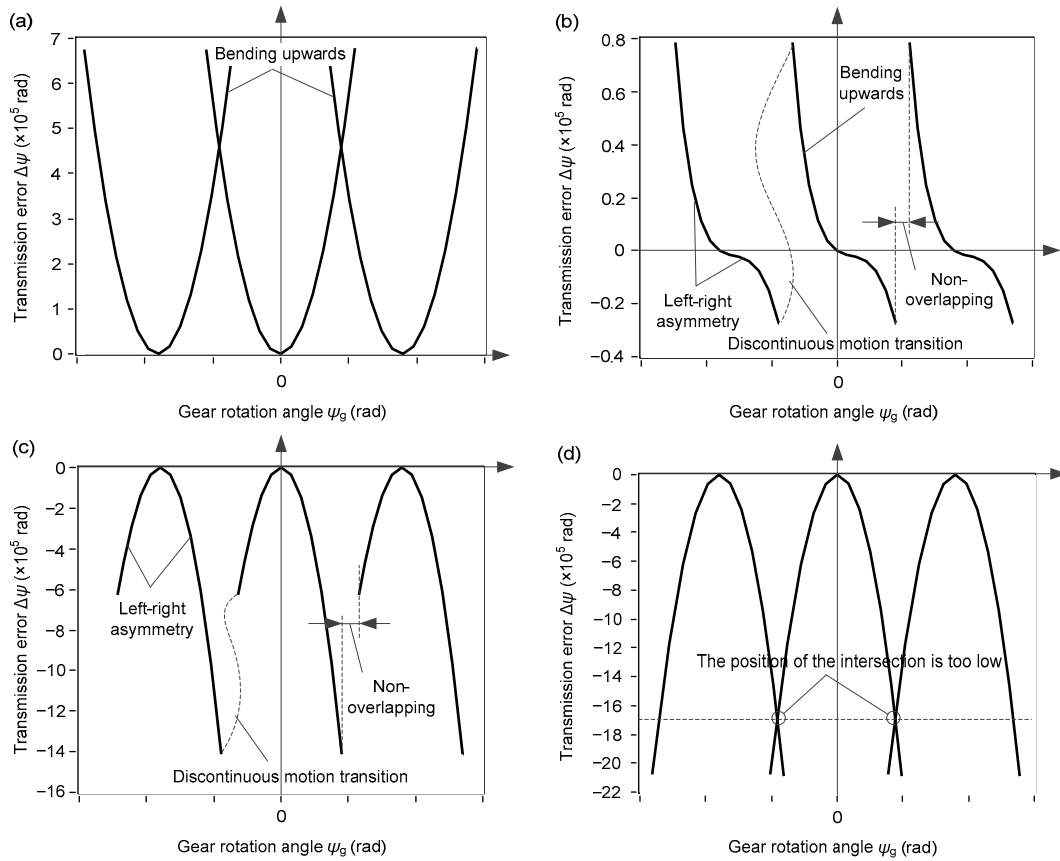


Fig. 1 Common defects of transmission error

(a) Both sides bending upwards; (b) One side bending upwards; (c) No intersection; (d) The position of the intersection is too low

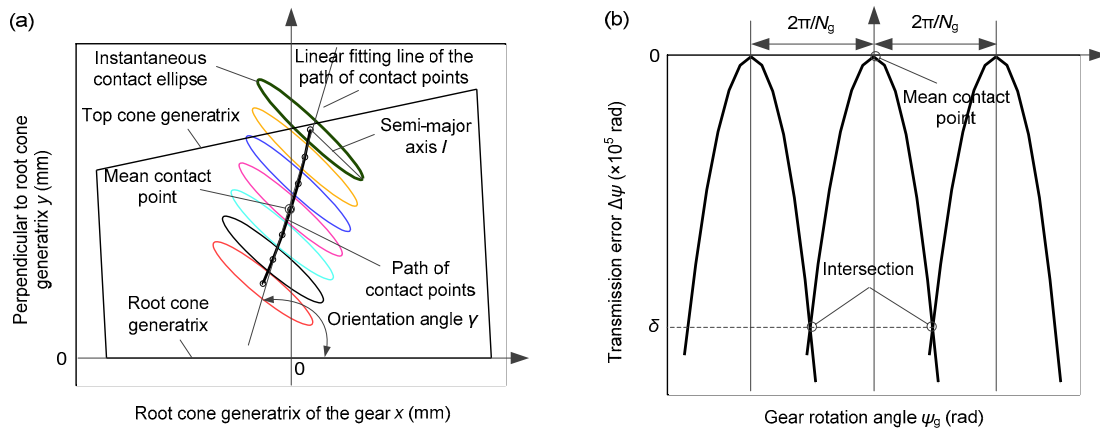


Fig. 2 Optimization objectives

(a) Contact pattern of the gear tooth surface; (b) Transmission error curve (N_g is the number of teeth in the gear)

semi-axes is different. Therefore, l can be represented as the mean value

$$l = \frac{\sum_{k=0}^{n-1} l_k}{n}, \quad (2)$$

where l_k is the optimal value of the semi-major axis of the k th contact ellipse and n the number of instantaneous contact ellipses inside the cycle of meshing.

2. Orientation angle of contact path γ

The orientation angle γ is defined as the angle between the contact path and the root cone generatrix of the gear. It can prevent the defects of inner opposite angular contact, outer opposite angular contact, and non-overlapping transmission error curves. For a spiral bevel gear drive, the convex and concave sides of a pinion tooth are in mesh with the concave and convex sides of the gear, respectively. In the case of the convex side of the gear, there is no intersection in the transmission error curve if γ is less than zero. When γ is greater than zero, the overlapping portion of the transmission error curve increases with the increase of γ , which means that the contact ratio of the gear drive increases. Nonetheless, an overlarge γ leads to severe inner opposite angular contact and a requirement for extremely high accuracy of assembly of the gear drive. In the case of the concave side of the gear, the situation is reversed. Hence, the optimal value of γ can be chosen as

$$\gamma_{\text{OPT}} \in \begin{cases} [50^\circ, 70^\circ], & \text{for convex side,} \\ [110^\circ, 130^\circ], & \text{for concave side.} \end{cases} \quad (3)$$

Thus, γ influences both the contact pattern and the transmission error curve. Although γ can restrict the defects of non-overlapping transmission error curves, it cannot effectively prevent the defect of no intersection. The path of contact points can be represented as its linear fitting line:

$$\text{Pa}_y(\text{Pa}_x) = \sum_{i=0}^1 c_i^\gamma (\text{Pa}_x)^i, \quad (4)$$

where Pa_x and Pa_y are the x - and y -coordinates of the contact point, respectively, and c_i^γ is the i th power coefficient of the function of contact path. Hence, γ

can be represented as

$$\gamma = \arctan c_1^\gamma. \quad (5)$$

3. Intersection ordinate of the transmission error curve δ

The intersection ordinate δ can effectively restrain the shape of the transmission error curve and prevent the defects of bending upwards, non-overlapping, no intersection, left-right asymmetry, and low position of intersection. Note that δ should be negative, and its absolute value must be as small as possible so that the real transmission ratio can get close enough to the theoretical value $i=N_g/N_p$ (N_g and N_p are the numbers of teeth of the gear and the pinion, respectively). Nonetheless, an extremely small absolute value of δ will lead to the emergence of the defect of bending upwards. Hence, the optimal value of δ can be chosen as

$$\delta_{\text{OPT}} = (-6 \sim -4) \times 10^{-5}. \quad (6)$$

It is difficult to obtain the analytical expression of the transmission error curve, and therefore it can be represented as its polynomial function:

$$\Delta\psi(\psi_g) = \sum_{i=0}^4 c_i^\delta (\psi_g)^i, \quad (7)$$

where c_i^δ is the i th power coefficient of the function of transmission error curve.

Hence, δ can be represented as

$$\delta = c_0^\delta + c_2^\delta \left(\frac{\pi}{N_g} \right)^2 + c_4^\delta \left(\frac{\pi}{N_g} \right)^4. \quad (8)$$

4 Control parameters

The gear machine-tool settings are considered as known so that the gear surface S_g is already determined. Therefore, the expected contact pattern and transmission error depend entirely on the pinion surface S_p . In other words, the conditions of meshing and contact are determined by the pinion cutting parameters. A spiral gear drive is a special case of a

hypoid gear drive, in which the offset $E=0$. Therefore, we focus on the study of a hypoid gear drive.

4.1 Pitch cone parameters of a hypoid gear drive

The geometrical relationships of the pitch cone parameters of a hypoid gear drive are illustrated in Fig. 3.

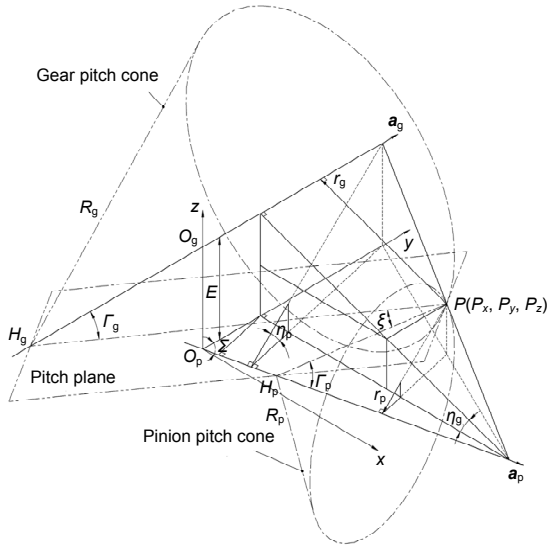


Fig. 3 Geometrical relationships of pitch cone parameters of a hypoid gear drive

a_g and a_p are the unit axial vectors of the gear and the pinion, respectively; H_g and H_p are the pitch cone apexes of the gear and the pinion, respectively; O_g and O_p are the ideal intersections of the gear and the pinion, respectively; P is the pitch point of the hypoid gear drive; P_x , P_y , and P_z are the x -, y -, and z -coordinates of the pitch point, respectively; r_g and r_p are the pitch circle radii of the gear and the pinion, respectively; R_g and R_p are the pitch cone distances of the gear and the pinion, respectively; Γ_g and Γ_p are the pitch angles of the gear and the pinion, respectively; ξ is the offset angle of the hypoid gear drive; Σ is the shaft angle of the hypoid gear drive; η_g and η_p are the offset angles of the gear and the pinion, respectively; E is the offset

In general, the offset E and the shaft angle Σ are regarded as given. Assume that in the rectangular coordinate system $\sigma_{O_p}=\{O_p; x, y, z\}$, the coordinates (P_x, P_y, P_z) of the pitch point P are known. The unit axial vector of the pinion a_p is in the x - y plane, and the unit axial vector of the gear a_g is parallel to the x - y plane and y -axis. Then all the other pitch cone parameters can be represented as follows:

$$\tan \eta_p = \frac{P_z}{P_y \sin \Sigma - P_x \cos \Sigma}, \quad (9)$$

$$\tan \eta_g = \frac{E - P_z}{P_x}, \quad (10)$$

$$r_p = \frac{P_z}{\sin \eta_p}, \quad (11)$$

$$\tan \Gamma_g = \left(\frac{E \cot \eta_p}{\sin \Sigma} - P_y \right) / r_g, \quad (12)$$

$$\tan \Gamma_p = \left[\frac{E \cos \eta_g}{\sin \Sigma} - \frac{P_x}{\sin \Sigma} + (P_y - P_x \cot \Sigma) \cos \Sigma \right] / r_p, \quad (13)$$

$$R_p = \frac{r_p}{\sin \Gamma_p}, \quad (14)$$

$$R_g = \frac{r_g}{\sin \Gamma_g}, \quad (15)$$

$$\sin \xi = \frac{\sin \Sigma \sin \eta_g}{\cos \Gamma_p}. \quad (16)$$

The longitudinal shape of the tooth in the pitch plane is the curve of the intersection of the tooth surface (Fig. 4). The longitudinal shapes of the gear and the pinion are tangent at the pitch point P , which is the origin of the rectangular coordinate system $\sigma_P=\{P; x, y, z\}$. The x -axis is in the pitch plane and tangent to the longitudinal shape. The z -axis is perpendicular to the pitch plane and along the line crossing both axes of the gear and the pinion. The mean spiral angles β_g and β_p are formed by the x -axis and the generatrix of the pitch cones of the gear and the pinion, respectively, which pass through P .

The relationship between the mean spiral angles and the offset angle ξ (Fig. 4) can be represented as

$$\beta_p = \beta_g + \xi. \quad (17)$$

The unit axial vectors a_p and a_g are represented in σ_P as

$$a_p = \begin{bmatrix} \cos \Gamma_p \cos \beta_p \\ \cos \Gamma_p \sin \beta_p \\ \sin \Gamma_p \end{bmatrix}, \quad (18)$$

$$\mathbf{a}_g = \begin{bmatrix} \cos \Gamma_g \cos \beta_g \\ \cos \Gamma_g \sin \beta_g \\ -\sin \Gamma_g \end{bmatrix}. \quad (19)$$

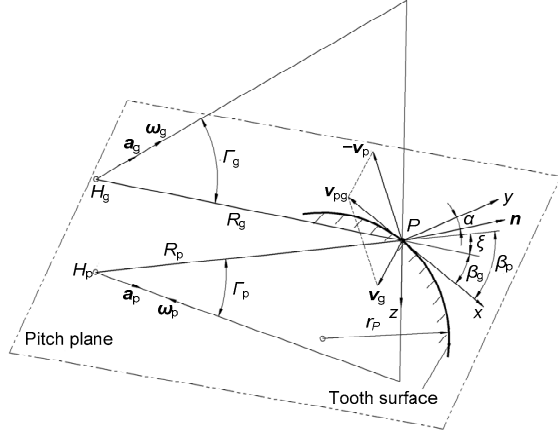


Fig. 4 Spiral angle and pressure angle of the hypoid gear drive

\mathbf{n} is the unit normal vector of contact point of the gear and the pinion; r_p is the curvature radius of tooth trace at the pitch point; \mathbf{v}_g and \mathbf{v}_p are the velocity vectors of point P of the gear and the pinion, respectively; \mathbf{v}_{pg} is the relative velocity vector of point P of the pinion with respect to the gear; α is the pressure angle; ω_g and ω_p are the angular velocity vectors of the gear and the pinion, respectively; \mathbf{a}_g and \mathbf{a}_p are the unit axial vectors of the gear and the pinion, respectively; H_g and H_p are the pitch cone apexes of the gear and the pinion, respectively; R_g and R_p are the pitch cone distances of the gear and the pinion, respectively; Γ_g and Γ_p are the pitch angles of the gear and the pinion, respectively; ξ is the offset angle of the hypoid gear drive; P is the pitch point of the hypoid gear drive; β_g and β_p are mean spiral angles formed by the x -axis and the generatrix of the pitch cones of the gear and the pinion, respectively

Assume that the angular velocity vector of the gear is $\omega_g = \omega_g \mathbf{a}_g$. Therefore, the angular velocity vector of the pinion is $\omega_p = -(N_g/N_p)\omega_g \mathbf{a}_p$. The velocity \mathbf{v}_g is represented by

$$\mathbf{v}_g = \omega_g \times \overline{H_g P}. \quad (20)$$

Similarly, the velocity \mathbf{v}_p is represented as

$$\mathbf{v}_p = \omega_p \times \overline{H_p P}. \quad (21)$$

The relative velocity of point P of the pinion with respect to the gear is represented by

$$\mathbf{v}_{pg} = \mathbf{v}_p - \mathbf{v}_g = \omega_g \begin{bmatrix} -\frac{N_g}{N_p} r_p \sin \beta_p + r_g \sin \beta_g \\ \frac{N_g}{N_p} r_p \cos \beta_p - r_g \cos \beta_g \\ 0 \end{bmatrix}. \quad (22)$$

The pressure angle is formed by \mathbf{n} (the unit common normal vector of the gear and the pinion tooth surfaces in the y - z plane (Fig. 4)) and the pitch plane. Hence, \mathbf{n} can be calculated as

$$\mathbf{n} = \begin{bmatrix} 0 \\ \cos \alpha \\ \sin \alpha \end{bmatrix}. \quad (23)$$

According to the equation of meshing $\mathbf{v}_{pg} \cdot \mathbf{n} = 0$, the following equation can be obtained:

$$\frac{N_g}{N_p} = \frac{r_g \cos \beta_g}{r_p \cos \beta_p}. \quad (24)$$

Plugging Eq. (24) into Eq. (17), and after formula transformation, β_g and β_p can be calculated as

$$\tan \beta_g = \left(\cos \xi - \frac{N_p r_g}{N_g r_p} \right) / \sin \xi. \quad (25)$$

Two other critical pitch cone parameters, i.e., limit pressure angle α_L and limit curvature radius r_L , can be calculated, respectively (Shtipelman, 1978; Zeng, 1989):

$$-\tan \alpha_L = \frac{R_p \sin \beta_p - R_g \sin \beta_g}{R_p \tan \Gamma_p + R_g \tan \Gamma_g} \cdot \frac{\tan \Gamma_p \tan \Gamma_g}{\cos \xi}, \quad (26)$$

$$\frac{1}{r_L} = \frac{1}{\tan \beta_p - \tan \beta_g} \left[-\tan \alpha_L \left(\frac{\tan \beta_p}{R_p \tan \Gamma_p} + \frac{\tan \beta_g}{R_g \tan \Gamma_g} \right) + \frac{1}{R_p \cos \beta_p} - \frac{1}{R_g \cos \beta_g} \right]. \quad (27)$$

Above all, if the coordinates (P_x, P_y, P_z) of the pitch point P are given, all the other pitch cone parameters can be obtained. In other words, three

independent parameters can uniquely and exactly determine all the other pitch cone parameters of a hypoid gear drive. In addition, with E , Σ , N_p , and N_g , there are only seven independent pitch cone parameters of a hypoid gear drive.

4.2 Relative curvatures of a hypoid gear drive

There is a linear contact between conjugate tooth surfaces of the gear and the pinion of the theoretical hypoid gear drive, and the contact line with point P is illustrated in Fig. 5. Having a linear contact, the conjugate tooth surfaces of the gear and the pinion envelope each other by their relative movement.

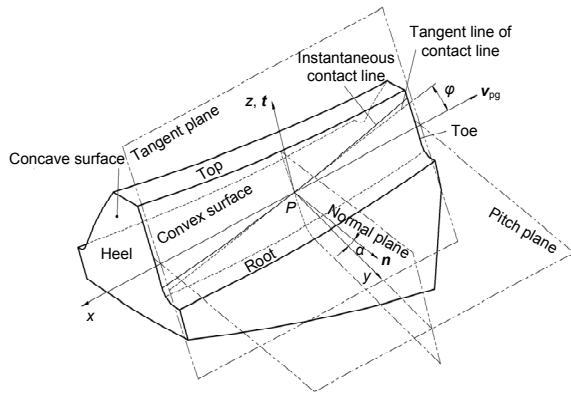


Fig. 5 Instantaneous contact line of the theoretical hypoid gear drive

t is the unit vector of tooth depth; φ is the orientation angle of the instantaneous contact line; P is the pitch point of the hypoid gear drive; n is the unit normal vector of contact point of the gear and the pinion; α is the pressure angle; v_{pg} is the relative velocity vector of point P of the pinion with respect to the gear

In the rectangular coordinate system σ_P , the x - and z -axes (or t) are defined as the directions of the tooth trace and tooth depth, respectively (Fig. 5). The relative curvatures of the gear and the pinion at point P can be represented as

$$\begin{cases} \Delta A = A_g - A_p, \\ \Delta B = B_g - B_p, \\ \Delta C = C_g - C_p, \end{cases} \quad (28)$$

where A_g and A_p are the principal curvatures of tooth trace of the gear and the pinion, B_g and B_p are the principal curvatures of tooth depth of the gear and the

pinion, C_g and C_p are the geodesic torsions of tooth trace of the gear and the pinion, respectively, ΔA is the relative principal curvature of tooth trace of the gear and the pinion, ΔB is the relative principal curvature of tooth depth of the gear and the pinion, and ΔC is the relative geodesic torsion of the tooth trace of the gear and the pinion.

It is clear from Fig. 5 that the contact line can be defined by angle φ between its tangent line and the relative velocity vector v_{pg} in the tangent plane. For the linear contact (Zeng, 1989; Wu, 2009), the relative curvatures of conjugate surfaces satisfy:

$$\Delta A \Delta B - (\Delta C)^2 = 0, \quad (29)$$

$$\tan \varphi = -\frac{\Delta C}{\Delta B}. \quad (30)$$

If the curvature radius of the gear at the contact point r_p and the relative geodesic torsion of tooth trace C_g are known, φ can be calculated as follows (Shtipelman, 1978; Zeng, 1989):

$$\tan \varphi = \frac{R_p \tan \Gamma_p R_g \tan \Gamma_g}{R_p \tan \Gamma_p + R_g \tan \Gamma_g} \cdot \frac{1}{1+u} \left[\left(\frac{\tan \beta_p}{R_p \tan \Gamma_p} + \frac{\tan \beta_g}{R_g \tan \Gamma_g} \right) \sin \alpha - \left(\frac{1}{R_p \cos \beta_p} - \frac{1}{R_g \cos \beta_g} - \frac{\tan \beta_p - \tan \beta_g}{r_p} \right) \cos \alpha \right], \quad (31)$$

$$\Delta B = \left(\frac{1}{R_p \tan \Gamma_p} + \frac{1}{R_g \tan \Gamma_g} \right) (1+u)^2 \left/ \left\{ \left(\frac{\tan \beta_g}{R_p \cos \beta_p} - \frac{\tan \beta_p}{R_g \cos \beta_g} \right) \cos \alpha - \left[\sin \alpha + (1+u) \tan \varphi \tan \xi \right] \cdot \frac{\cos \xi}{\cos \beta_p \cos \beta_g} \left(\frac{1}{R_p \tan \delta_p} + \frac{1}{R_g \tan \delta_g} \right) \right\} \right., \quad (32)$$

where

$$u = \frac{R_p \tan \Gamma_p R_g \tan \Gamma_g}{R_p \tan \Gamma_p + R_g \tan \Gamma_g} \cdot (\tan \beta_p - \tan \beta_g) C_g, \quad (33)$$

$$r_p = -\cos \alpha / A_g. \quad (34)$$

Eqs. (28)–(34) show the relationships between pitch cone parameters and curvature parameters of a hypoid gear drive. We conclude that the curvature parameters $A_g, B_g, C_g, A_p, B_p,$ and C_p can be converted into pitch cone parameters φ and ΔB . Under the precondition of knowing all the pitch cone parameters, there are six equations and three unknowns, and therefore there are only three independent curvature parameters of a hypoid gear drive.

4.3 Determination of pinion tooth surface

Machine-tool settings, including machine-tool adjustment parameters and the cutter blade profile, determine the tooth surface. Adjustment parameters are related to the pitch cone parameters while the cutter blade profile is related to curvature parameters. The influence of the cutter blade profile has been studied by many researchers, and is not discussed in this study, so curvature parameters of the generating gear are taken as given.

A pinion combines with a gear and a generating gear to form a theoretical hypoid gear drive. In the case of pinion and gear, all seven independent pitch

cone parameters ($E, \Sigma, N_p, N_g, \beta_p, r_g,$ and r_L) and three independent curvature parameters ($A_g, B_g,$ and C_g) are known. Hence, the values of $\beta_p, \Gamma_p, R_p, A_p, B_p,$ and C_p can be obtained from Eqs. (9)–(34). In the case of pinion and generating gear, all six independent curvature parameters ($A_g, B_g, C_g, A_p, B_p,$ and C_p) are known, and can be converted into the two pitch cone parameters φ and ΔB . In regular calculations of the machine parameters, N_p and Σ are known. Therefore, the only uncertain pitch cone parameters are E and N_g , which can be determined accurately by φ and ΔB , and be obtained by the iterative method. This is the main principle for calculating the machine-tool settings of a hypoid gear drive.

In theory, $\beta_p, \Gamma_p, R_p, A_p, B_p,$ and C_p can all be chosen as control parameters for optimal design. However, the first three relate to the wheel body rather than the tooth profile. Therefore, in this study, $A_p, B_p,$ and C_p are selected as control parameters. This complies with the principle that meshing characteristics are determined mainly by the curvatures of the tooth surfaces. The iterative method for calculating pinion machine-tool settings is summarized in Fig. 6.

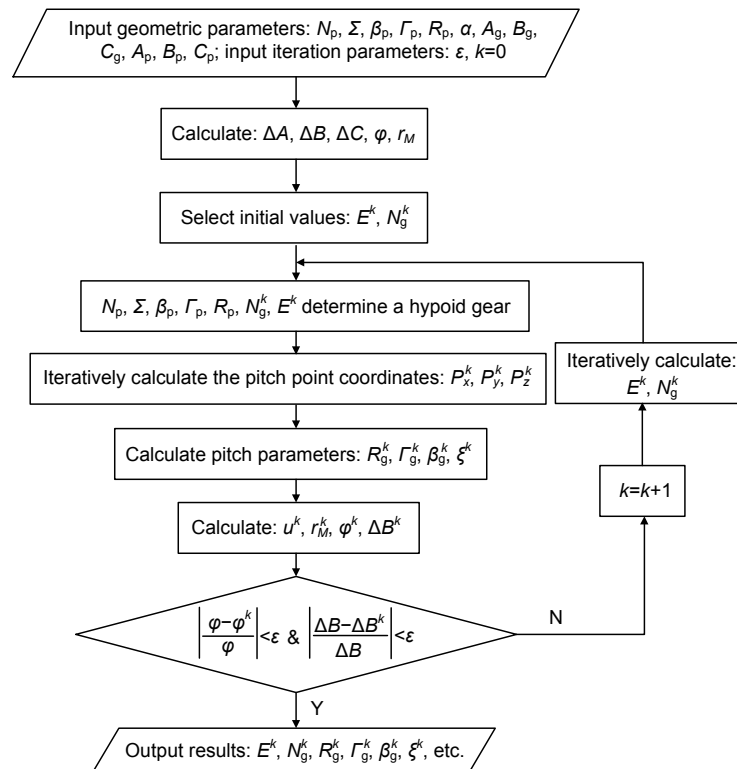


Fig. 6 Iterative method for calculating pinion machine-tool settings

5 Optimization algorithm

5.1 Optimization goal equation

There are three optimization objectives: l_{OPT} , γ_{OPT} , and δ_{OPT} . Obviously, to achieve the overall optimization goal, l , γ , and δ should reach their target values respectively. Therefore, the global optimization equation is set up as follows:

$$\begin{aligned} \min f(l, \gamma, \delta) = & \max \left\{ \left| \frac{l - l_{OPT}}{l_{OPT}} \right|, \varepsilon \right\} \\ & + \max \left\{ \left| \frac{\gamma - \gamma_{OPT}}{\gamma_{OPT}} \right|, \varepsilon \right\} + \max \left\{ \left| \frac{\delta - \delta_{OPT}}{\delta_{OPT}} \right|, \varepsilon \right\}. \end{aligned} \quad (35)$$

The equation $f(l, \gamma, \delta) = 3\varepsilon$ indicates that the overall optimization goal has been obtained.

5.2 Feasible region of contact point

The position of the contact point M should be in the range of the tooth surfaces of the gear and the pinion. Otherwise, the contact point M is false, as well as its corresponding transmission error curve. A false contact point M would reduce the precision of the calculation of l , γ , and δ ; hence, should be avoided.

The tooth surfaces of the gear and the pinion are the feasible region of the contact point M (Fig. 7). Assuming the areas of the tooth surfaces of the gear and the pinion are ΔS_g and ΔS_p , respectively, in axial planes of the gear and the pinion, the relation for a real contact point M is

$$\begin{cases} \Delta S_g^{\text{top}} + \Delta S_g^{\text{toe}} + \Delta S_g^{\text{root}} + \Delta S_g^{\text{heel}} = \Delta S_g, \\ \Delta S_p^{\text{top}} + \Delta S_p^{\text{toe}} + \Delta S_p^{\text{root}} + \Delta S_p^{\text{heel}} = \Delta S_p, \end{cases} \quad (36)$$

where ΔS^{top} is the area of triangle delimited by contact point M and top line, ΔS^{toe} the area of triangle delimited by contact point M and toe line, ΔS^{root} the area of triangle delimited by contact point M and root line, and ΔS^{heel} the area of triangle delimited by contact point M and heel line.

If the contact point is out of the range of the gear tooth surface, then the relation is

$$\Delta S_g^{\text{top}} + \Delta S_g^{\text{toe}} + \Delta S_g^{\text{root}} + \Delta S_g^{\text{heel}} > \Delta S_g. \quad (37)$$

Similarly, if the contact point is out of the range of the pinion tooth surface, the relation is

$$\Delta S_p^{\text{top}} + \Delta S_p^{\text{toe}} + \Delta S_p^{\text{root}} + \Delta S_p^{\text{heel}} > \Delta S_p. \quad (38)$$

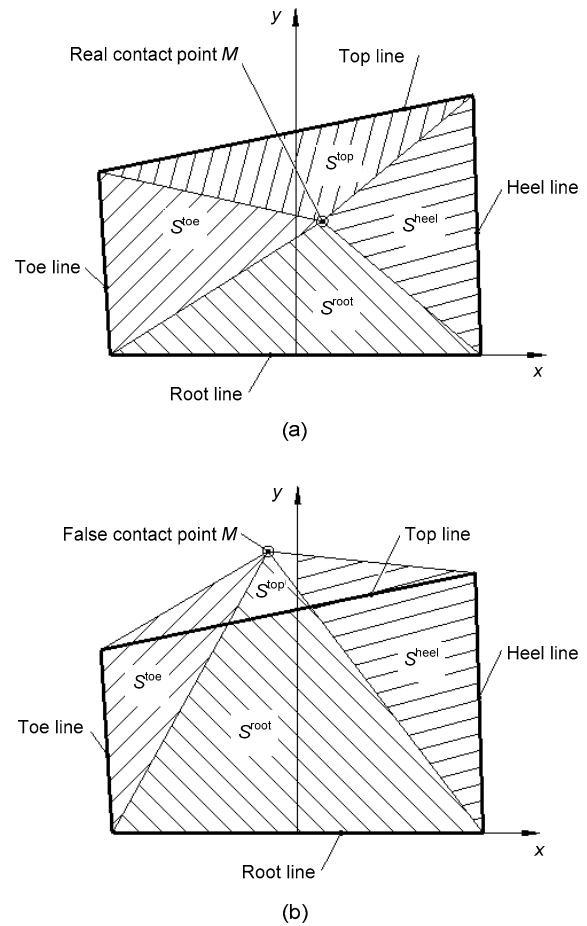


Fig. 7 Feasible region of contact point
(a) Real contact point; (b) False contact point

5.3 Solution of optimization equation

In this study, a complex-constrain genetic algorithm is used to solve the above global optimization equation of tooth contact pattern and transmission error. A genetic algorithm (Zhuo and Zhou, 2015; Zhang et al., 2016) is a search heuristic that imitates the process of natural selection. Genetic algorithms generate solutions to optimization problems using techniques of inheritance, mutation, selection, and crossover. However, the new individuals generated by a genetic algorithm have a certain randomness, which

may exceed the feasible region. To compensate for this limitation, a complex method is used to constrain the new individuals. The concrete procedure of this method is shown in Fig. 8.

6 Case studies and discussion

6.1 Case studies

To verify the feasibility of the above optimization method of tooth contact pattern and transmission error, as well as to analyze the effect of each control parameter on the optimization goal, a hypoid gear drive is chosen for the case studies. Its basic geometric parameters are listed in Table 1.

Gear convex surface and pinion concave surface are the main working tooth surfaces of a hypoid gear

Table 1 Basic geometric parameters of the hypoid gear drive

Geometrical parameter	Description	
	Pinion	Gear
Number of teeth	9	35
Hand of spiral	Left-hand	Right-hand
Module (mm)	4.899	4.899
Shaft angle (°)	90	90
Offset (mm)	44.45	44.45
Heel pitch circle diameter (mm)	64.913	171.45
Pitch angle (°)	13.695	72.863
Tooth width (mm)	38.41	26.92
Mean spiral angle (°)	50	15.63

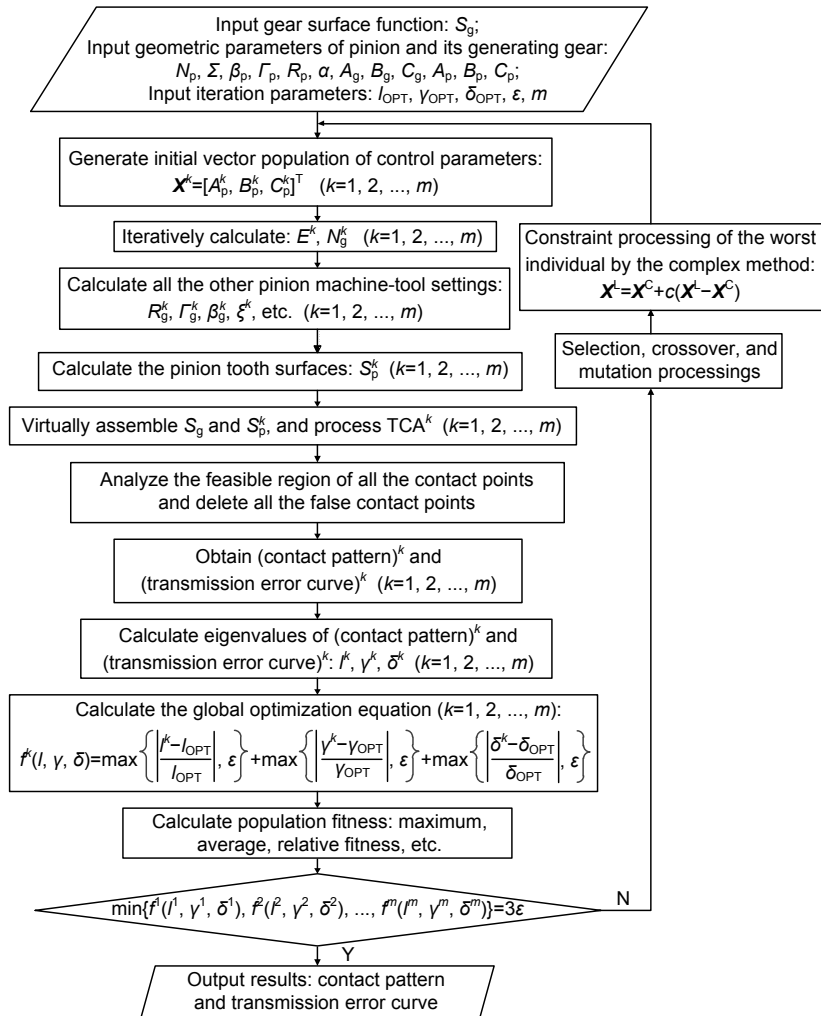


Fig. 8 Solution procedure of the optimization equation of tooth contact pattern and transmission error

c is the coefficient; m is the number of population of iterative computation; X^C , X^L , and X^k are the mean, worst individual, and the k th values of vector population, respectively; ε is the computation precision

drive; therefore, we choose them as the case studies and the optimization processes of their contact pattern and transmission error curves are as shown in Fig. 9.

The optimization goals are $l_{OPT}=4$ mm, $\gamma_{OPT}=60^\circ$, and $\delta_{OPT}=-5\times 10^{-5}$ rad, and the computation precision is $\varepsilon=0.001$ (Fig. 9). The iterative processing

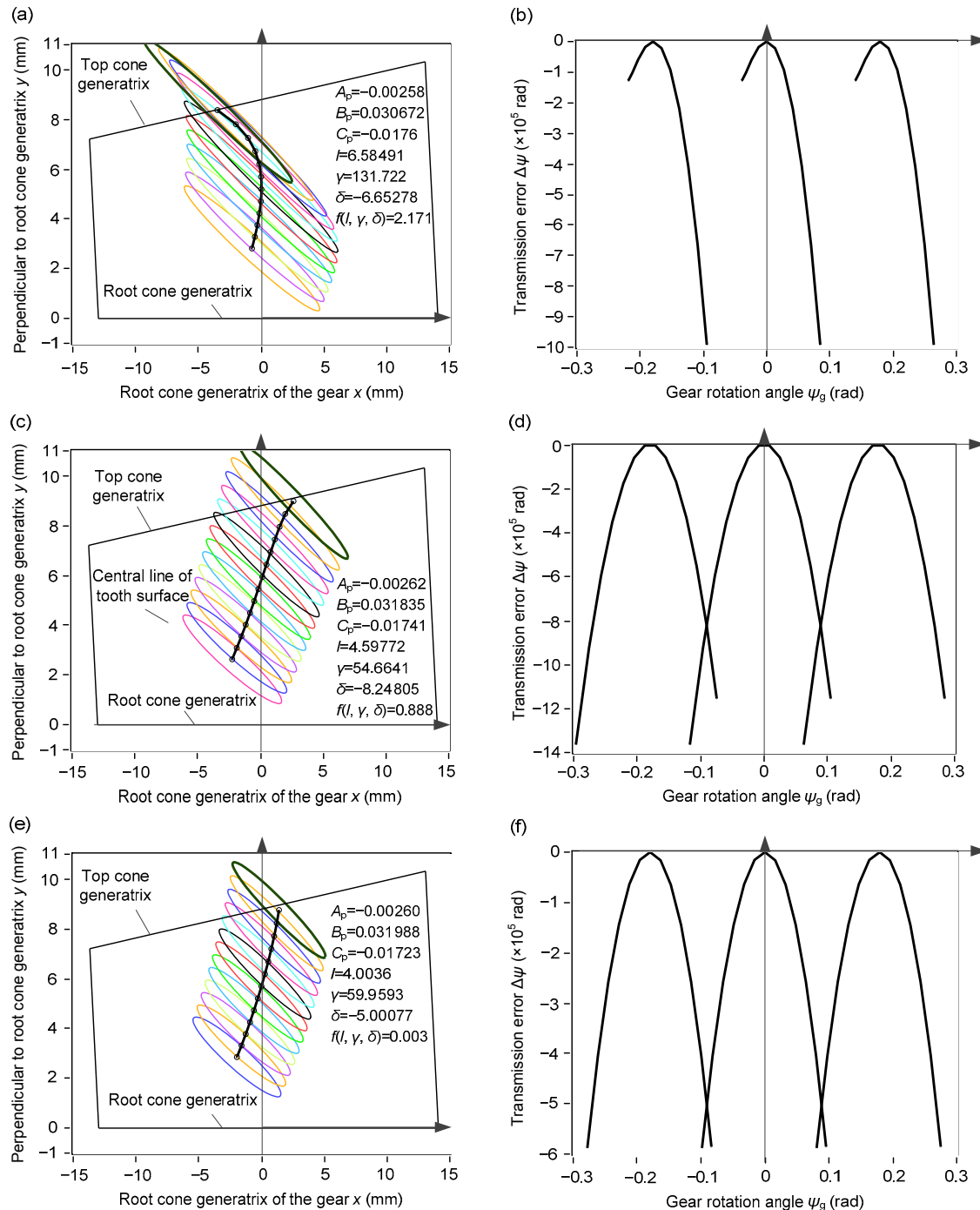


Fig. 9 Optimization processes for the tooth contact patterns and transmission error curves of the gear convex and the pinion concave faces

(a) Initial value of tooth contact pattern; (b) Initial value of transmission error curve; (c) Intermediate value of tooth contact pattern; (d) Intermediate value of transmission error curve; (e) Result value of tooth contact pattern; (f) Result value of transmission error curve

has achieved the expected optimization goal and has good convergence. This indicates that the optimization objectives, the control parameters, and the optimization algorithm are well matched. Finally, the optimized 3D path of the contact points and contact ellipses are shown in Fig. 10.

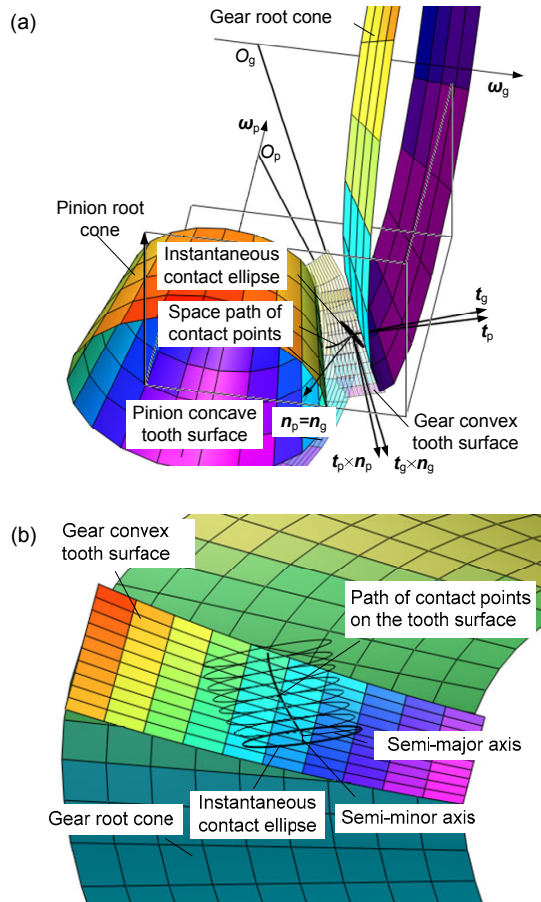


Fig. 10 Optimized 3D path of contact points and contact ellipses

(a) Contact pattern of the gear drive; (b) Contact pattern of the gear tooth surface. n_g and n_p are the unit normal vectors of contact point of the gear and the pinion, respectively; t_g and t_p are the unit vectors of tooth depth of the gear and the pinion, respectively; ω_g and ω_p are the angular velocity vectors of the gear and the pinion, respectively; O_g and O_p are the ideal intersections of the gear and the pinion, respectively

6.2 Correlations between optimization objectives and control parameters

From the above optimization processes, as well as case studies of a gear concave surface and a pinion

convex surface (not shown here due to space constraints), the following relationships between the three optimal objectives (l , γ , δ) and the three control parameters (A_p , B_p , C_p) can be obtained:

1. A_p is related mainly to l , and l generally increases with the increase of $|A_p|$.

2. B_p is related mainly to γ , and γ generally decreases with the increase of $|B_p|$.

3. C_p is related mainly to δ , and δ generally increases with the increase of $|C_p|$.

The above shows the effect of only a single control parameter on a single optimization objective. However, the relationship between the three control parameters and the three optimization objectives is nonlinear. The interactive influences among the control parameters are so complicated that a numerical iteration method is needed to solve the optimization equation.

7 Finite element analysis

7.1 Model of the drive system

The application of finite element analysis (FEA) to analyze the contact characteristics of spiral and hypoid bevel gears has become an important research direction in recent years. To verify the above optimal results, the finite element model (FEM) of a simplified hypoid gear drive system has been established and its quasi-static meshing characteristics analyzed with FEM software ABAQUS (Fig. 11).

7.2 Contact pattern

Fig. 12 shows the effect of torque load T_g on the contact pattern of the gear convex face. There is a good agreement between the FEM loaded contact pattern and the above mathematical optimization result ($T_g=0$) when T_g is small, which verifies the correctness of the optimization method. With the increase of T_g , the area of the instantaneous contact region and the length of the contact path increase, while γ decreases. This illustrates that the torque load is a very important factor in determining the actual contact pattern. With the increase of T_g , the contact region expands to the tooth heel and hardly expands to the tooth toe. Therefore, in practical application, to make full use of the bearing capacity of the whole tooth face, the mounting position of the gear drive

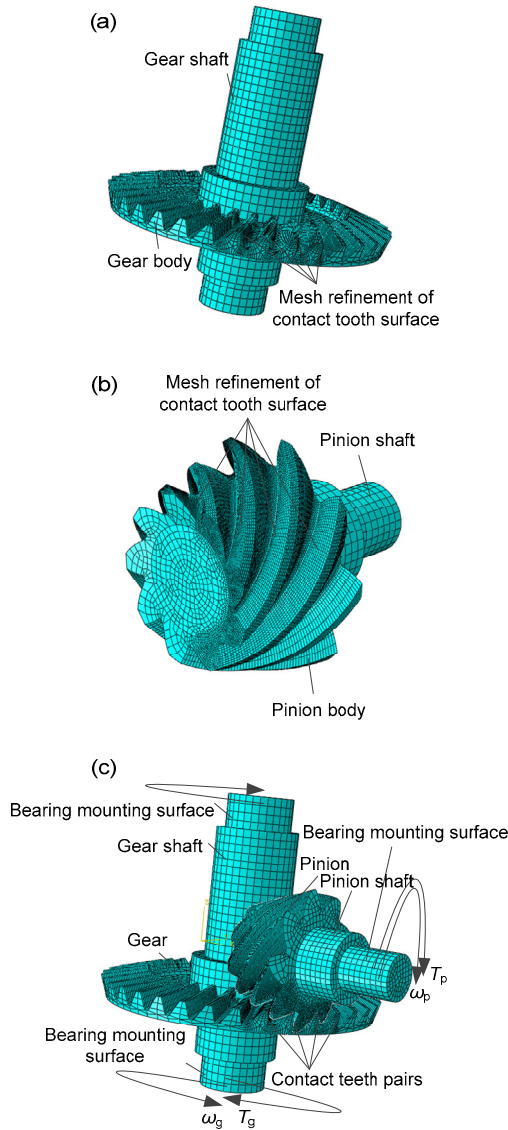


Fig. 11 Finite element model of the simplified hypoid gear drive system

(a) Gear; (b) Pinion; (c) Drive system. T_g and T_p are the torque loads of the gear and input torque of the pinion, respectively; ω_g and ω_p are the angular velocities of the gear and the pinion, respectively

should reach the lightly loaded contact region near the tooth toe; then with the increase of load, the contact region would naturally expand to the tooth heel. These analysis results are consistent with those in Shtipelman (1978) and Zeng (1989).

7.3 Transmission error

Fig. 13 shows the effect of torque load T_g on the transmission error of the gear drive. The maximum

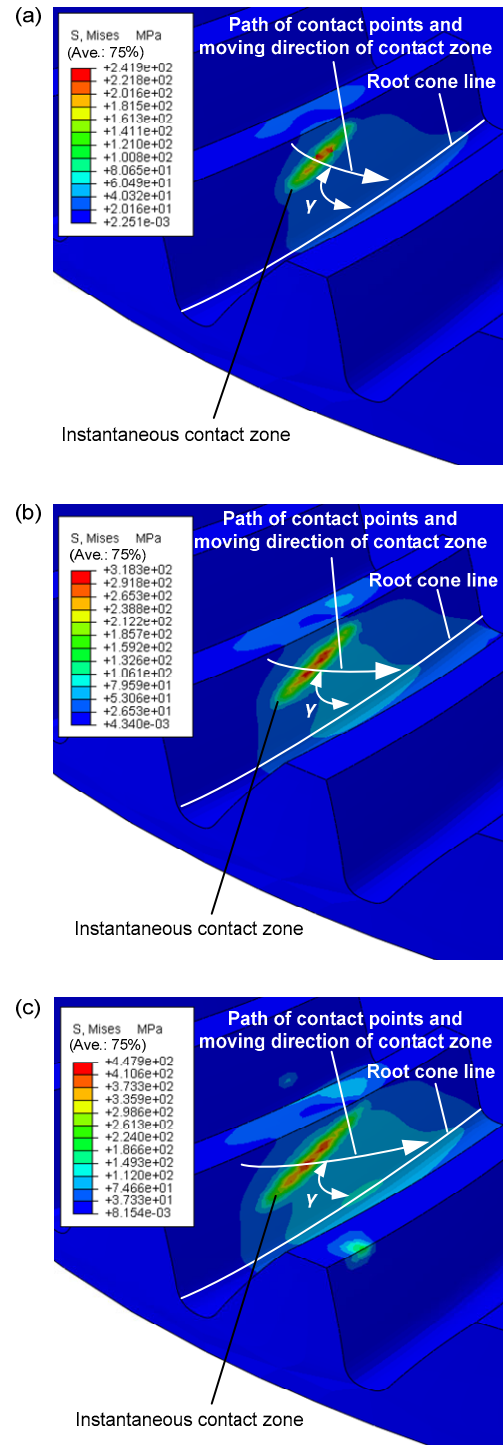


Fig. 12 Loaded contact pattern of the gear convex face

(a) $T_g=100$ N·m; (b) $T_g=200$ N·m; (c) $T_g=400$ N·m

value of the loaded transmission error is lower than $|\delta_{OPT}|$ when T_g is small, which again confirms the correctness of the optimization method.

Unlike the theoretical transmission error curve, the loaded transmission error curve is continuous, and its oscillation period is $2\pi/N_g$ (Fig. 13a). When T_g is small, the meshing state of the gear drive is single or double teeth-meshing. Therefore, there are two fluctuation areas of the curve in a cycle, which represent the motion transition from single to double teeth-meshing and double to single teeth-meshing, respectively. The oscillation amplitude of the curve increases with the increase of T_g . This can be explained by the increasing deformation of the components of the drive system with the increase of T_g . If T_g rises further, at $T_g=400$ N·m, the meshing state becomes double or three teeth-meshing. In this case, though the maximum of the transmission error has increased (larger than $|\delta_{OPT}|=5\times 10^{-5}$ rad), the motion transition has become smoother and the curve does not contain obvious fluctuation areas. This may be because the actual contact ratio of the gear drive increases.

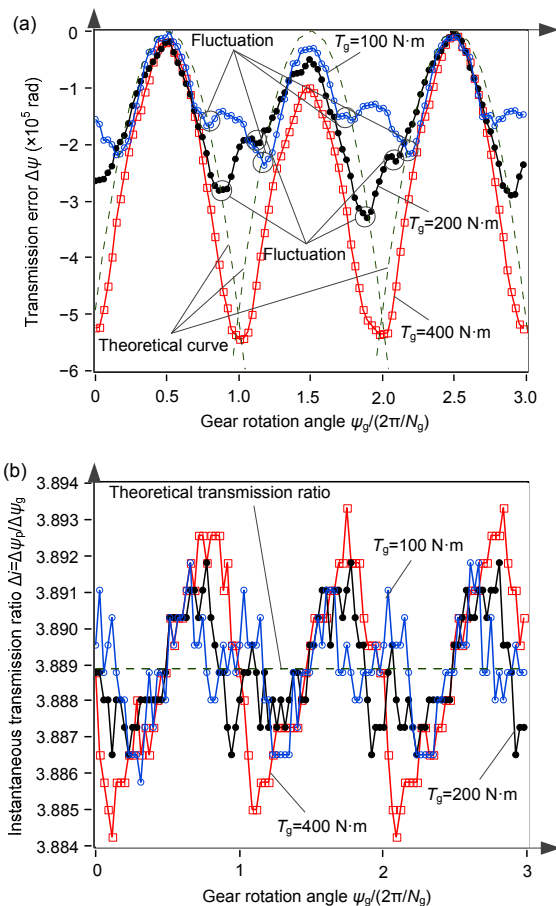


Fig. 13 Loaded transmission error curve (a) and instantaneous transmission ratio (b) of the gear drive

The instantaneous transmission ratio $\Delta i = \Delta\psi_p/\Delta\psi_g$ fluctuates up and down near the theoretical value (Fig. 13b). The oscillation amplitude of Δi changes little when T_g is small. However, if T_g rises further, the amplitude increases with the increase of T_g , which means that the stability of the gear drive transmission decreases. This could be due to the increase in loaded deformations of the gear drive and the shafts.

8 Conclusions

A global optimization methodology for tooth contact pattern and transmission error of spiral bevel and hypoid gears has been presented, which includes three optimization objectives (l , γ , and δ), three control parameters (A_p , B_p , and C_p), and the complex-constrain genetic algorithm solving method. A hypoid gear drive was chosen for case studies. The results have verified that the methodology can obtain the expected optimization objectives and has good convergence. Furthermore, the FEM of a simplified hypoid gear drive system was established and its quasi-static meshing characteristics analyzed. The results confirm the correctness of the optimization method. The major innovative aspects of this paper are as follows:

1. Three optimization objectives (l , γ , and δ) were selected to restrict most of the common defects, and the optimal values and the method for calculating the optimization objectives were presented.
2. A new set of fundamental equations for pitch cone parameters of a hypoid gear drive were established, as well as the relationships between pitch cone parameters and curvature parameters.
3. Three control parameters (A_p , B_p , and C_p) were selected to determine the pinion tooth surface, and an iterative method for calculating pinion machine-tool settings was presented.
4. A global optimization equation was established, and a complex-constrain genetic algorithm method for solving the optimization equation was presented.
5. Case studies of a hypoid gear drive indicated that the optimization objectives, the control parameters, and the optimization algorithm were well

matched, and correlations between the optimization objectives and the control parameters were discussed.

6. An FEM of the hypoid gear drive system was established and its quasi-static meshing characteristics were analyzed. The results verified the correctness of the optimization method.

7. With the increase of T_g , the area of the contact region and the length of the contact path increased, γ decreased, and the contact region expanded to the tooth heel and hardly to the tooth toe.

8. With the increase of T_g , the oscillation amplitude of the transmission error and instantaneous transmission ratio increased, as well as the actual contact ratio.

References

- Achtmann, J., Bär, G., 2004. Optimized bearing ellipses of hypoid gears. *Journal of Mechanical Design*, **125**(4): 739-745.
<http://dx.doi.org/10.1115/1.1625403>
- Argyris, J., Fuentes, A., Litvin, F.L., 2002. Computerized integrated approach for design and stress analysis of spiral bevel gears. *Computer Methods in Applied Mechanics and Engineering*, **191**(11-12):1057-1095.
[http://dx.doi.org/10.1016/S0045-7825\(01\)00316-4](http://dx.doi.org/10.1016/S0045-7825(01)00316-4)
- Artoni, A., Bracci, A., Gabiccini, M., et al., 2008. Optimization of the loaded contact pattern in hypoid gears by automatic topography modification. *Journal of Mechanical Design*, **131**(1):011008.
<http://dx.doi.org/10.1115/1.3013844>
- Artoni, A., Kolivand, M., Kahraman, A., 2009. An ease-off based optimization of the loaded transmission error of hypoid gears. *Journal of Mechanical Design*, **132**(1): 011010.
<http://dx.doi.org/10.1115/1.4000645>
- Guo, W., Mao, S., Yang, Y., et al., 2016. Optimization of cutter blade profile for face-hobbed spiral bevel gears. *The International Journal of Advanced Manufacturing Technology*, **85**(1):209-216.
<http://dx.doi.org/10.1007/s00170-015-7893-5>
- Litvin, F.L., Fuentes, A., 2004. Gear Geometry and Applied Theory (2nd Edition). Cambridge University Press, Cambridge, UK, p.627.
- Litvin, F.L., Wang, A.G., Handschuh, R.F., 1998. Computerized generation and simulation of meshing and contact of spiral bevel gears with improved geometry. *Computer Methods in Applied Mechanics and Engineering*, **158**(1-2):35-64.
[http://dx.doi.org/10.1016/S0045-7825\(97\)00229-6](http://dx.doi.org/10.1016/S0045-7825(97)00229-6)
- Litvin, F.L., Fuentes, A., Fan, Q., et al., 2002. Computerized design, simulation of meshing, and contact and stress analysis of face-milled formate generated spiral bevel gears. *Mechanism and Machine Theory*, **37**(5):441-459.
[http://dx.doi.org/10.1016/S0094-114X\(01\)00086-6](http://dx.doi.org/10.1016/S0094-114X(01)00086-6)
- Litvin, F.L., Fuentes, A., Hayasaka, K., 2006. Design, manufacture, stress analysis, and experimental tests of low-noise high endurance spiral bevel gears. *Mechanism and Machine Theory*, **41**(1):83-118.
<http://dx.doi.org/10.1016/j.mechmachtheory.2005.03.001>
- Mermoz, E., Astoul, J., Sartor, M., et al., 2013. A new methodology to optimize spiral bevel gear topography. *CIRP Annals — Manufacturing Technology*, **62**(1):119-122.
<http://dx.doi.org/10.1016/j.cirp.2013.03.067>
- Shtipelman, B.A., 1978. Design and Manufacture of Hypoid Gears. John Wiley & Sons, New York, USA.
- Simon, V.V., 2009a. Design and manufacture of spiral bevel gears with reduced transmission error. *Journal of Mechanical Design*, **131**(4):041007.
<http://dx.doi.org/10.1115/1.3087540>
- Simon, V.V., 2009b. Head-cutter for optimal tooth modifications in spiral bevel gears. *Mechanism and Machine Theory*, **44**(7):1420-1435.
<http://dx.doi.org/10.1016/j.mechmachtheory.2008.11.007>
- Simon, V.V., 2013. Design of face-hobbed spiral bevel gears with reduced maximum tooth contact pressure and transmission errors. *Chinese Journal of Aeronautics*, **26**(3):777-790.
<http://dx.doi.org/10.1016/j.cja.2013.05.005>
- Simon, V.V., 2014. Optimization of face-hobbed hypoid gears. *Mechanism and Machine Theory*, **77**:164-181.
<http://dx.doi.org/10.1016/j.mechmachtheory.2014.02.003>
- Vogel, O., Griewank, A., Bär, G., 2002. Direct gear tooth contact analysis for hypoid bevel gears. *Computer Methods in Applied Mechanics and Engineering*, **191**(36):3965-3982.
[http://dx.doi.org/10.1016/S0045-7825\(02\)00351-1](http://dx.doi.org/10.1016/S0045-7825(02)00351-1)
- Wu, X.T., 2009. Gear Engagement Principle (2nd Edition). Xi'an Jiaotong University Press, Xi'an, China (in Chinese).
- Zeng, T., 1989. Spiral Bevel Gear Design and Processing. Harbin Institute of Technology Press, Harbin, China (in Chinese).
- Zhang, T.T., Huang, W., Wang, Z.G., et al., 2016. A study of airfoil parameterization, modeling, and optimization based on the computational fluid dynamics method. *Journal of Zhejiang University-SCIENCE A (Applied Physics & Engineering)*, **17**(8):632-645.
<http://dx.doi.org/10.1631/jzus.A1500308>
- Zhuo, Y., Zhou, X., 2015. Dynamic characteristic analysis of high-speed spherical ball bearing. *Journal of Mechanical Engineering*, **51**(5):37-46 (in Chinese).

中文概要

题目：一种螺旋锥齿轮齿面接触区和传动误差的全局优化方法

目的：传统的齿面接触分析技术存在调整参数繁多、控制目标不明确和不包含传动误差优化等缺陷。本

文旨在提出一种齿面接触区和传动误差的全局优化设计方法,以得到满足齿轮传动性能要求的小轮产形轮节锥参数及机床调整参数。

创新点: 1. 提出了新的确定各节锥参数之间几何关系的计算公式,并建立了节锥参数与曲率参数的相关公式; 2. 提出以齿面接触区长半轴、接触线方向角和传动误差曲线交点纵坐标为优化目标,以齿面法曲率和短程挠率为控制参数,以复合形法约束处理的遗传算法为求解途径的齿面接触特性全局优化设计方法。

方法: 1. 分析常见齿面接触区和传动误差曲线的缺陷及其原因(图 1); 2. 提出全局优化目标(图 2),

进行节锥参数和曲率参数分析,从而确定控制参数(图 3~6),建立优化方程并进行求解算法分析(图 7和 8),然后进行实例计算分析(图 9和 10); 3. 建立齿轮副传动系统有限元分析模型,验证优化方法的正确性(图 11~13)。

结论: 1. 优化设计的实例分析表明,优化目标、控制参数和优化算法具有良好的匹配性; 2. 通过优化目标与控制参数的相关性分析,得出了控制参数的影响特征; 3. 通过有限元分析验证,优化设计结果达到了预期的齿轮传动性能指标。

关键词: 螺旋锥齿轮; 齿面接触; 传动误差; 优化设计; 遗传算法; 有限元分析